KfK 3641
Dezember 1983

Pattern Selection in Single-Component Systems Coupling Bénard Convection and Solidification

S. H. Davis, U. Müller, C. Dietsche
Institut für Reaktorbauelemente

Kernforschungszentrum Karlsruhe

KERNFORSCHUNGSZENTRUM KARLSRUHE
Institut für Reaktorbauelemente

KfK 3641

Pattern Selection in Single-Component Systems Coupling Bénard Convection and Solidification

S.H. Davis*), U. Müller, C. Dietsche

*) Department of Engineering Sciences and Applied Mathematics, Northwestern University, Evanston Illinois 60201, USA

Kernforschungszentrum Karlsruhe GmbH, Karlsruhe

Kernforschungszentrum Karlsruhe GmbH
ISSN 0303-4003

Abstract

A horizontal layer is heated from below and cooled from above so that the enclosed single-component liquid is frozen in the upper part of the layer. When the imposed temperature difference is such that the Rayleigh number across the liquid is supercritical, there is Bénard convection coupled with the dynamics of the solidification interface. An experiment is presented which shows that the interfacial corrugations that result are two-dimensional when this "ice" is thin but hexagonal when the "ice" is thick. A weakly-nonlinear convective instability theory is presented which explains this behavior, and isolates the mechanism of the pattern selection. Jump behavior is seen in the liquid-layer thickness at the onset of hexagonal convection.

Musterauswahl in einkomponentigen Systemen bei Kopplung von Bénard Konvektion mit Gefriervorgängen

Zusammenfassung

Eine horizontale einkomponentige Flüssigkeitsschicht wird an der Unterseite erwärmt und an der Oberseite derart gekühlt, daß der obere Teil der Schicht gefriert. Wenn die an die Schicht angelegte Temperaturdifferenz einen kritischen Wert überschreitet, resultiert in dem flüssigen Teil der Schicht eine Bénard Konvektion, die mit den Gefriervorgängen an der Eisoberfläche gekoppelt ist. Es wird ein Experiment vorgestellt, das die Verformung der Eisfläche unter der Wirkung der Bénard Konvektion zeigt. Die resultierenden Verformungen haben zweidimensionalen Charakter, wenn die Eisschicht dünn ist, nehmen jedoch hexagonalen Charakter bei dicken Eisschichten an. Es wird eine schwach nichtlineare Instabilitätstheorie vorgestellt, welche dieses Verhalten des Systems einschließlich der Auswahl der Muster an der Gefrierfläche erklärt. Es wird ein sprunghaftes Anwachsen der Schichthöhe der Flüssigkeit bei Beginn der Konvektion mit hexagonaler Zellform von der Theorie vorhergesagt.

Contents

1. Introduction

Convection can be the dominant mode of heat and mass transport in many processes that involve the freezing or melting of material. Such is the case for the freezing of ponds or bays and the storage of thermal energy based on the melting of the storage material. The solidification in molds of liquid metals or alloys and the growth of crystals from melt or aqueous solutions are cases where double-diffusive processes may be present so that there is the need to understand the interaction in multicomponent systems. Although the effect of convective transport in all these processes has been a subject of many experimental and theoretical investigations (see e.g. Foster (1969), Farhadieh and Tankin (1975), Fischer (1981), Saitoh and Hirose (1980. 1982), Hurle & Jakeman (1981), Marshall (1981)) fundamental uncertainties exist in the prediction of the progress and the shape of the freezing or melting front. The growth of crystals from binary solutions is a process where the interaction of adverse temperature and concentration gradients may generate unwanted interfacial instabilities during a unidirectional solidification (Mullins & Sekerka (1964), Coriell et al.(1980), Coriell and Sekerka (1982), Hurle & Jakeman (1983)). These instabilities generally deform the initially planar solid-liquid interface and lead to a cellular pattern of micro-segregation. The interaction of the temperature and concentration field near a progressing solidification front gives rise to the so-called morphological instability (Mullins & Sekerka 1964) in which convective effects are negligible. Weakly nonlinear theories (Wollkind & Segel (1970), Wollkind & Raissi (1974), Sriranganathan et al.(1983)) lead to prediction of hexagonal patterns for the resulting interfacial corrugations.

Interfacial instabilities may also originate from the onset of solutal or thermal convection in the liquid phase if the gradients are parallel to the gravity vector. Stability criteria based on linear analyses for solutal driven convection have been given for various conditions by Hurle, Jakeman & Wheeler (1982, 1983). They also analyse the complex system of interacting morphological

instabilities and solutal convection and show that stationary and oscillatory (overstable) perturbations of the temperature, concentration and velocity may occur when the critical conditions are exceeded.

In the present work we wish to focus on systems in which thermal convection and corrugations of a freezing/melting interface are strongly coupled. We consider a horizontal layer of a single component liquid, cyclohexane, which is transparent, has no anomolous physical properties near its freezing point and whose thermal variations in physical properties are negligible. The layer is heated from below and the boundary temperature adjusted so that the upper part is frozen and there is a solid-liquid interface. Depending on the Rayleigh number of the liquid, the heat in the liquid is transferred either by conduction only or by conduction and convection. The natural convection generally will occur in cellular form as it is observed in Benard convection. If the heat is transported uniformly by conduction only the interface between the solid and liquid layer will be planar; however it will become corrugated, if natural convection occurs in the liquid. The situation is sketched in figure 1.

Work on related systems is scarce. Yen (1980) performs experiments on melting ice blocks underneath or above a heated horizontal layer of water. He finds regular patterns of corrugations at the ice surface. When the ice block is melted from below, he observes an array of small "inverted hemispherical cells" at the ice surface. A pattern of axisymmetric troughs and crests occur at the ice surface when the ice block is melted from above. No explanation is given for the occurrence of the different shapes of the interface deflections. The density anomaly of water at 4 ^{o}C may have had a major influence on the pattern formation. Pantaloni et al. (1977) have obtained hexagonal planforms of solid-liquid interfaces in Rayleigh-Bénard experiments conducted with molten salts. They attribute the appearance of such patterns to the strong thermal variations of the viscosity in the fluid layer close to the solidification front. Such non-Boussinesq effects have been shown by Busse (1967) to give rise to hexagonal convec-

tion in uncoupled systems. Pantaloni et al. (1977) imply that the convective pattern in the liquid generates the hexagonal corrugations at the solid-liquid interface.

It is the aim of the present investigation to identify the patterns of convective flow and interfacial corrugation, determine the parametric ranges in which different patterns occur and study the basic mechanics of the interfacial-flow interactions. In section 2 we report on experiments which identify the corrugations of the interface. In section 3 we perform a weakly nonlinear analysis of the coupled convective/interfacial system. We compare the theory and experiment and explain the mechanism of the pattern selection and the observations of the experiments. In section 4 we summary the study.

2. Experiments

2.1 Apparatus and Procedure

The test apparatus is displayed schematically in figure 2. The test volume is confined at the lower and upper side by square copper plates of 287x287 mm^2 surface each. The side walls consist of 5 mm thick glass plates. The distance between the horizontal plates is varied by placing small ceramic spacers of low heat conductivity at the rim of the plates. Spacers of height 4.18 mm and 5.04 mm are employed in the experiments. The manufacturing tolerances of both flatness of the copper plates and the spacer heights is less than $\pm$0.02 mm. For temperature control the copper plates are put in direct contact to a system of meandering cooling channels at their lower and upper sides respectively. Coolant is provided from two high precision thermostats of temperature variance $\Delta T = \pm 0.01^{\circ}C$. The whole test chamber including the connecting pipes to the thermostats is insulated against external temperature perturbations by styrofoam plates and rubber foam hoses.

For measuring the temperatures at the horizontal boundaries two Ni-Cr-Ni thermocouples are positioned in the upper copper plate and one in the lower plate, each 0.2 mm beneath the surface adjacent to the test volume. The same zero point thermostat serves as a reference instrument for all thermocouples. Temperature fluctuations of less than $\pm 0.01\ ^{\circ}C$ are assured. The thermoelectric voltage is amplified by difference amplifiers by a factor 1000 and displayed by a digital voltmeter.

Before starting the actual tests the thermocouples are calibrated by correlating the signals to the melting temperature of the test liquid, cyclohexane. The properties of this liquid are listed in table 1. The calibration is performed by first reducing the temperature at the upper copper plate until a thin layer of solidified material of less than 0.1 mm is formed at the surface. We shall hereafter call this solid "ice". Then the temperature is slowly raised until only a few tiny patches of "ice" are seen on

the surface. During this process the temperature of the lower copper plate is kept constant at 6.9 °C. An equivalent procedure is used for calibrating the thermocouple in the lower plate. This calibration is essential for obtaining the two main measured quantities, the temperature differences $T_o - T_s$ and $T_s - T_1$.

Cyclohexane is chosen as the test liquid since the material properties are well known and no anomalies in material properties exist in the range 3 °C and 8°C where the experiments have been carried out. Moreover, cyclohexane is transparent and exhibits a fixed melting temperature.

The structure of the solid-liquid interface, i.e. the "ice" surface, is directly visualized through observation slits at all four glass side walls. The reflection of the "ice" structure by the polished surface of the lower copper plate of mirror quality is an essential aid for the direct observation. However, for a photographic documentation the upper copper plate is removed from the test apparatus at certain fixed temperature levels of the lower and upper plate. Photos are then taken of the corrugated "ice" surface under favorable lighting conditions. The removal of the plate has to be rapid in order to avoid unwanted sublimation of the cyclohexane or condensation of air humidity at the "ice" surface. Typically, photographs were taken between 30 and 60 seconds after the start of the dismantling of the insulation of the apparatus.

2.2 Observations

We shall relate our observations to the case of pure heat conduction in which the solid-liquid interface is planar and its position is at $z = h_L$. This state is analyzed in Section 3 where we find that

$$\frac{h-h_L}{h_L} = \frac{\lambda^{(S)}}{\lambda^{(L)}} \frac{T_s-T_1}{T_o-T_s} \equiv B \ . \qquad (2.1)$$

Here $\lambda^{(S)}$ and $\lambda^{(L)}$ are the thermal conductivities for the solid

and liquid, respectively, and for small B, B turns out to be the equivalent Biot number for the heat transfer from the liquid to the solid. Notice that B also measures the amount of "ice" present.

We also inroduce the Rayleigh number R to measure convection in the liquid. Here

$$R = \alpha g \frac{(T_o - T_s) h_L^3}{\kappa^{(L)} \nu} , \qquad (2.2)$$

where α is the volume expansion coefficient, g is the magnitude of the gravitational acceleration, $\kappa^{(L)}$ is the thermal diffusivity and ν is the kinematic viscosity.

In all experiments we keep T_o fixed so that the temperature difference $T_o - T_s$ is fixed and we vary the temperature T_1 of the upper boundary. Thus, unlike the classical experiments in Bénard convection, the Rayleigh number is varied through changes in h_L, not through changes in the temperature difference.

Each experiment begins with a value of T_1 giving convection in the liquid. T_1 is then reduced in small steps. When T_1 reaches a value where the "ice" surface becomes planar, the state of pure conduction has replaced the state of convection. From here the experimental run is reversed by increasing the temperature T_1 in small increments keeping T_o fixed until the initial state of convection is reached again.[1] Different experimental runs lasted typically between 2 and 4 weeks. The rates of stepwise change of the temperature at the upper plate was 0.5 K/min, the state of each measuring point was at least stationary for 90 minutes before the data were taken.

Photographs of corrugated "ice" surfaces are shown in figure 3. Depending on the thickness of the "ice" layer, different patterns occur. If the "ice" layer is very thin, i.e. about 0.1 mm or less, line patterns appear as shown in figure 3a. A hexagonal pattern is generated for "ice" layers whose thicknesses are comparable to the depth of the liquid layer as shown in figure 3c.

1) In temperature ranges where qualitative changes in the flow behavior were expected the monotonic variations in the temperature T_1 were supplemented by cyclic variations in order to fix the temperature threshold of transitions.

In an intermediate range both polygonal and line patterns were observed to coexist as displayed in figure 3b.

The different states realized during two runs of experiments are shown in the graph of figure 4. Each state is characterized by two parameters, the Rayleigh number R and the Biot number B. For the upper curve the total layer depth h is 5.04 mm, whereas for the lower curve h = 4.18 mm. The range of different patterns of the "ice" surface is characterized by the parameter B. We find two-dimensional line patterns for $B < 0.05$ and hexagonal patterns for $B > 0.16$. For the intermediate range $0.05 < B < 0.16$ a mixed pattern of lines and polygons is observed. The particular experimental trajectories shown by the experiments is due to the fact that variations in T_1 in the experiment cause both the Rayleigh number and the Biot number to vary simultaneously. Generally the different states could also be arranged under the condition of a constant Rayleigh number though the temperatures at both copper plates would have to be varied appropriately. As mentioned before, for reasons of experimental convenience, only the temperature of the upper copper plate was actually changed.

An analysis of the experimental errors has shown that the values B for the transition between the different "ice" patterns are accurate within the following bounds:

$0.02 < B < 0.08$, line pattern/mixed pattern transition
$0.13 < B < 0.19$, mixed pattern/hexagonal pattern transition.

Our experimental observations lead to a physical mechanism for the generation of the patterns of corrugation that couple convective flow with interface deflection.

If the Rayleigh number of the liquid layer exceeds a critical value, cellular convection starts enhancing the heat transfer in the liquid layer. This results in partial melting of the "ice" when the critical conditions are moderately exceeded. Since the convection cells are characterized by zones of up-flow and down-flow, the "ice" melting is not uniform. More "ice" is melted near

the zones where warmer fluid rises toward the interface compared to zones where cold fluid sinks towards to lower boundary. This effect is displayed schematically in figure 1. It results in a formation of crests and troughs at the "ice" surface as observed in figure 3.

The surface deflection can lead to a sufficient degree of vertical asymmetry that hexagonal convection can be created as shown by Davis and Segel (1968) for fluid-fluid interfaces. Our experimental observations indicate that this is the case when B is large. When B is small enough we see only line patterns. We next outline a theory based on these ideas.

3. Theoretical Model and Analysis

3.1 Formulation

Consider the configuration sketched in figure 1 where the horizontal parallel plates at $z = 0$ and $z = h$ have infinite horizontal extent. The lower plate at $z = 0$ is fixed at the temperature $T = T_0$ while the upper plate at $z = h$ is fixed at temperature $T = T_1$. The material between the plates is single component liquid if $T > T_s$ and its solid if $T < T_s$. The layer is heated from below in that $T_1 < T_s < T_0$ and there is a solid-liquid interface at $z = \eta$ with $0 < \eta < h$. The material properties are the density ρ_0, the specific heat c_p, the thermal conductivity λ, diffusivity κ, kinematic viscosity ν, and the volume expansion coefficient α; superscripts S and L will be used to designate solid and liquid properties when required.

The coupled effects of buoyancy-driven convection and phase changes will be described by thermal conduction in the solid and the Boussinesq equations (Mihaljian 1962) in the liquid. At the interface at $z = \eta$, we assume that there is no undercooling so that

$$T^{(L)} = T_s, \quad T^{(S)} = T_s. \tag{3.1}$$

The jump in heat flux is balanced by the production of latent heat L,

$$\rho_o^{(S)} L \, \eta_t = \left[\lambda^{(S)} \nabla T^{(S)} - \lambda^{(L)} \nabla T^{(L)}\right] \cdot \underline{n} \tag{3.2}$$

where $\underline{n}$ is the unit normal vector to the interface

$$\underline{n} = (-\eta_x, -\eta_y, 1)(1 + \eta_x^2 + \eta_y^2)^{-\frac{1}{2}} . \tag{3.3}$$

Subscripts x,y,z,t represent partial differentiation. The interface is non-mobile but deformable so that there is the kinematic condition

$$\rho_o^{(L)} \, \underline{v} \cdot \underline{n} = \left[\rho_o^{(S)} - \rho_o^{(L)}\right] (1 + \eta_x^2 + \eta_y^2)^{-\frac{1}{2}} \eta_t \tag{3.4}$$

and the no slip condition

$$\underline{v} \cdot \underline{t}^{(1)} = \underline{v} \cdot \underline{t}^{(2)} = 0 \tag{3.5}$$

where $\underline{t}^{(1)}$ and $\underline{t}^{(2)}$ are unit tangent vectors

$$\underline{t}^{(1)} = (1+\eta_y^2, -\eta_x\eta_y, \eta_x)(1+\eta_x^2+\eta_y^2)^{-\frac{1}{2}}(1+\eta_y^2)^{-\frac{1}{2}} \tag{3.6a}$$

$$\underline{t}^{(2)} = (0, 1, \eta_y)(1 + \eta_y^2)^{-\frac{1}{2}} . \tag{3.6b}$$

The governing system possesses a <u>static equilibrium solution</u> in which the interface is planar at $z = \eta = h_L$, the velocity vector $\underline{v}$ is identically zero, the pressure p is hydrostatic and the temperatures are purely conductive. Here,

$$\overline{T}^{(L)} = T_s - (T_o - T_s) \frac{z - h_L}{h_L} \tag{3.7a}$$

and

$$\overline{T}^{(S)} = T_s - (T_s - T_1) \frac{z - h_L}{h - h_L} . \tag{3.7b}$$

Fields (3.7) satisfy conditions (3.1), $T^{(S)} = T_1$ at $z = h$ and $T^{(L)} = T_o$ at $z = 0$. The flux condition (3.2) further constrains the parameters so that

$$\frac{h_S}{h_L} = \frac{\lambda^{(S)}}{\lambda^{(L)}} \frac{T_s - T_1}{T_o - T_s} \equiv B \tag{3.8}$$

where

$$h = h_S + h_L \ . \tag{3.9}$$

Thus, the thicknesses of the solid and liquid layers are determined by T_o, T_1 and T_S. In particular, as $B \to 0$, the solid disappears.

We now introduce the following scales:

$$\begin{aligned}
x,y,z \quad &\sim \quad h_L \ , \\
t \quad &\sim \quad h_L^{\,2}/\kappa^{(L)} \ , \\
u,v,w \quad &\sim \quad \hat{W} \equiv \left[\kappa^{(L)} \alpha g h_L \, (T_o - T_s)/\nu\right]^{\frac{1}{2}} \ , \\
p \quad &\sim \quad \nu \rho_o^{(L)} \hat{W}/h_L \ , \\
T - T_S \quad &\sim \quad T_o - T_s \ .
\end{aligned} \tag{3.10}$$

We use the same symbols as before to denote non-dimensional quantities; the full governing Boussinesq system is as follows:

$$T_t^{(L)} + R^{\frac{1}{2}} \underline{v} \cdot \nabla T^{(L)} = \nabla^2 T^{(L)} \ , \tag{3.11a}$$

$$P^{-1} \left[\underline{v}_t + R^{\frac{1}{2}} \underline{v} \cdot \nabla \underline{v}\right] = - \nabla p + \nabla^2 \underline{v} + R^{\frac{1}{2}} T^{(L)} \underline{k} \ , \tag{3.11b}$$

$$\nabla \cdot \underline{v} = 0 \quad , \tag{3.11c}$$

$$T_t^{(S)} = \kappa \nabla^2 T^{(S)} , \tag{3.11d}$$

$$\text{on } z = 0, \qquad \underline{v} = \underline{0}, \quad T^{(L)} = 1 \quad , \tag{3.11e}$$

$$\text{on } z = 1 + B, \qquad T^{(S)} = \lambda^{-1} B \quad , \tag{3.11f}$$

$$\text{on } z = \eta, \qquad \rho S \eta_t = \left[\lambda \nabla^{(S)} - \nabla T^{(L)} \right] \cdot \underline{n} \quad , \tag{3.11g}$$

$$T^{(L)} = T^{(S)} = 0 \quad , \tag{3.11h}$$

$$(\rho - 1)\left(1 + \eta_x^2 + \eta_y^2\right)^{-\frac{1}{2}} \eta_t = \underline{v} \cdot \underline{n} \quad , \tag{3.11i}$$

$$\underline{v} \cdot \underline{t}^{(1)} = \underline{v} \cdot \underline{t}^{(2)} = 0 \quad , \tag{3.11j}$$

where

$$\underline{k} = (0, 0, 1). \tag{3.12}$$

Here equations (3.11a,b,c) are the Boussinesq equations for the liquid and equation (3.11d) gives the thermal field in the solid. The following non-dimensional groups emerge:

$$R = \frac{\alpha g \left(T_o - T_s\right) h_L^{\,3}}{\kappa^{(L)} \nu} \quad , \tag{3.12a}$$

$$P = \frac{\nu}{\kappa^{(L)}} \quad , \tag{3.12b}$$

$$\rho = \frac{\rho_o^{(S)}}{\rho_o^{(L)}} \quad , \tag{3.12c}$$

$$\lambda = \frac{\lambda^{(S)}}{\lambda^{(L)}} \quad , \tag{3.12d}$$

$$\kappa = \frac{\kappa^{(S)}}{\kappa^{(L)}} \quad , \tag{3.12e}$$

$$S = \frac{\rho_o^{(L)} L \kappa^{(L)}}{\lambda^{(L)}(T_o - T_s)} \quad , \tag{3.12f}$$

$$B = \frac{\lambda^{(S)}}{\lambda^{(L)}} \frac{T_s - T_1}{T_o - T_s} \quad . \tag{3.12g}$$

The main parameters that govern steady convection in the present system are R and B. Notice that due to condition (3.8), a change in, say, T_1 causes both B and R to change simultaneously, the latter due to the variation in h_L.

In non-dimensional terms, the basic state has $\underline{v} = \underline{0}$, p hydrostatic and

$$\bar{T}^{(L)} = 1 - z \quad , \qquad 0 \leq z \leq 1 \; ; \tag{3.13a}$$

$$\bar{T}^{(S)} = \lambda^{-1}(1-z) \quad , \qquad 1 \leq z \leq 1+B \quad . \tag{3.13b}$$

3.2 Weakly Nonlinear Steady Convection

We wish to consider the basic state in which a slight rise in the temperature of the upper plate causes a slight melting of the solid. The increase in h_L, given that $T_o - T_s$ is fixed, causes the Rayleigh number to pass through its critical value R_c leading to steady cellular convection of amplitude ε. We seek to describe this weakly nonlinear steady convection using a perturbation theory first described by Malkus and Veronis (1958) by writing

$$\underline{v} = \underline{0} + \varepsilon \underline{v}_1 + \varepsilon^2 \underline{v}_2 + \cdots \quad , \tag{3.14a}$$

$$p = \overline{p} + \varepsilon p_1 + \varepsilon^2 p_2 + \cdots \quad , \tag{3.14b}$$

$$T^{(L)} = \overline{T}^{(L)} + \varepsilon T_1^{(L)} + \varepsilon^2 T_2^{(L)} + \cdots \quad , \tag{3.14c}$$

$$T^{(S)} = \overline{T}^{(S)} + \varepsilon T_1^{(S)} + \varepsilon^2 T_2^{(S)} + \cdots \quad , \tag{3.14d}$$

$$\eta = 1 \quad + \varepsilon\eta_1 \quad + \varepsilon^2 \eta_2 \quad + \cdots \tag{3.14e}$$

and representing

$$R = R_c + \varepsilon R_1 + \varepsilon^2 R_2 + \cdots \tag{3.15}$$

for all other parameters fixed. We substitute forms (3.14) and (3.15) into system (3.11) and equate to zero coefficients of like powers of ε.

At order unity we reobtain the basic state. At order ε we obtain the linear stability problem under neutral conditions. We separate variables using normal modes

$$(w_1, T_1^{(L)}, T_1^{(S)}, \eta_1) = (W_1(z), T_1^{(L)}(z), T_1^{(S)}(z), H_1)\Phi(x,y) \tag{3.16a}$$

where the planform function Φ satisfies

$$\Phi_{xx} + \Phi_{yy} = -k^2 \Phi \tag{3.16b}$$

and the usual normalization condition

$$\overline{\Phi^2} = 1 \quad . \tag{3.17}$$

Here the overbar denotes horizontal average over one period in x and y, i.e. over one cell and k is the overall wave number.

The temperature field in solid satisfies $\nabla^2 T_1^{(s)} = 0$ along with $T_1^{(S)}(x,y,1+B) = 0$ and $T_1^{(S)}(x,y,1) = \lambda^{-1}\eta$. We find that

$$T_1^{(S)}(z) = \lambda^{-1} H_1 \Lambda(\zeta) \tag{3.18}$$

where

$$\zeta = \frac{z-1}{B} \quad , \tag{3.19a}$$

and

$$\Lambda(\zeta) = \frac{\sinh k B (1-\zeta)}{\sinh k B} \quad . \tag{3.19b}$$

The linear stability problem in the liquid governs Bénard convection under neutral conditions:

$$(D^2-k^2)T_1^{(L)} + R^{\frac{1}{2}} W_1 = 0 \quad , \tag{3.20a}$$

$$(D^2-k^2)^2 W_1 - k^2 R^{\frac{1}{2}} T_1^{(L)} = 0 \quad , \tag{3.20b}$$

with

$$W_1(0) = DW_1(0) = T_1^{(L)}(0) = 0 \, , \tag{3.20c}$$

and

$$W_1(1) = DW_1(1) = DT_1^{(L)}(1) + T_1^{(L)}(1) = 0 \quad . \tag{3.20d}$$

Here $D = d/dz$ and

$$\mathcal{L} = - B^{-1} \left[\frac{d}{d\zeta} \Lambda(\zeta) \right]_{\zeta=0} = k \coth k B. \tag{3.21}$$

Note that the horizontal velocity components u_1 and v_1 can be written as

$$u_1 = \frac{1}{k^2} w_{1_{xz}} \, , \qquad v_1 = \frac{1}{k^2} w_{1_{yz}} \, . \tag{3.22}$$

The conditions (3.20d) show that at the onset of convection the solid-liquid interface behaves like a planar, rigid solid that is an <u>imperfect thermal conductor.</u> This thermal condition comes from the temperature and heat flux conditions (3.11g,h) linearized

about z = 1 . These have the form

$$T_1^{(L)}(1) = H_1 \tag{3.23a}$$

and

$$D\,T_1^{(L)}(1) = -\mathscr{L} H_1 . \tag{3.23b}$$

On the right-hand side of (3.23b) we have used solution (3.19). Notice that as $B \to 0$, $\mathscr{L}^{-1} \sim B$ so that the solid disappears and the interface becomes a perfect conductor. In this limit $DT_1(1) = O(1)$ and is bounded away from zero.

System (3.20) has a minimum critical Rayleigh number R_c which corresponds to $k = k_c$. In Figures 5 and 6 we plot these as functions of B as obtained by a straightforeward numerical integration. These are obtainable from the calculations of Nield (1968) even though we have a wave-number dependent "Biot" number $\mathscr{L}$. In all theory that follows we take $k = k_c$ for each given B.

It is easy to see that $DT_1(1) < 0$ so from equation (3.23b), we have $H_1 > 0$. Thus, there is a surface elevation ($H_1 > 0$) above a rising ($W_1 > 0$) convective current. This is consistent with the idea that the rising current is warm ($T_1 > 0$) so that it melts solid compared to its neighbors.

It is convenient in what follows to introduce a generalized notation for the description of disturbances in the liquid. We follow Davis and Segel (1968) and write the four-vector Ψ_i,

$$\underline{\Psi}_i = \begin{bmatrix} u_i \\ v_i \\ w_i \\ T_i^{(L)} \end{bmatrix} \tag{3.24a}$$

and the linear operators L and M,

$$\underline{\underline{L}} = \begin{bmatrix} \nabla^2 & o & o & o \\ o & \nabla^2 & o & o \\ o & o & \nabla^2 & o \\ o & o & o & \nabla^2 \end{bmatrix} \qquad (3.24b)$$

and

$$\underline{\underline{M}} = \begin{bmatrix} o & o & o & o \\ o & o & o & o \\ o & o & o & 1 \\ o & o & 1 & o \end{bmatrix}. \qquad (3.24c)$$

In terms of notation (3.24) the linear stability problem in the liquid written using the primative equations can be posed as follows:

$$\{\underline{\underline{L}} + R_c^{\frac{1}{2}} \underline{\underline{M}}\} \cdot \underline{\Psi}_1 - \begin{bmatrix} p_{1x} \\ p_{1y} \\ p_{1z} \\ 0 \end{bmatrix} = \underline{0} \quad , \qquad (3.25a)$$

$$\nabla \cdot \underline{v}_1 = 0 \quad . \qquad (3.25b)$$

If we pose the scalar product of two vectors Ψ_A and Ψ_B as

$$\langle \underline{\Psi}_A, \underline{\Psi}_B \rangle = \int_0^1 \overline{\left[u_A u_B + v_A v_B + w_A w_B + T_A^{(L)} T_B^{(L)}\right]} dz, \qquad (3.26)$$

then using the methods of Davis and Segel (1968), it is straightforeward to show subject to the present boundary conditions (3.20c,d), that system (3.25a,b) is self-adjoint. Note that these conditions are derived from

$$u_1 = v_1 = w_1 = T_1^{(L)} = 0 \quad \text{on} \quad z = 0 \tag{3.27a}$$

and

$$u_1 = v_1 = w_1 = T_{1z}^{(L)} + \mathcal{L} T_1^{(L)} = 0 \quad \text{on } z = 1. \tag{3.27b}$$

We now turn to the order ε^2 terms of the perturbation theory. In the solid, $\nabla^2 T_2^{(S)} = 0$ with $T_2^{(S)} = 0$ at $z = 1+B$ and $T_2^{(S)} = \lambda^{-1}\eta_2 - T_{1_z}^{(S)} \eta_1$ at $z = 1$. Thus,

$$T_2^{(S)}(z) = \{\lambda^{-1}\eta_2 - T_{1_z}^{(S)} \Big|_{z=1} \eta_1 \} \Lambda(\zeta) \tag{3.28}$$

and we find that the $O(\varepsilon^2)$ Stefan condition becomes

$$T_{2_z}^{(L)}(1) = -\mathcal{L}(\eta_2 + \mathcal{L}\eta_1^2). \tag{3.29}$$

Here we have used forms (3.18), (3.19), (3.21) and (3.28) as well as early relations on boundary conditions on the liquid at $z = 1$. Finally, we use $T_2^{(S)} - \lambda^{-1}\eta_2 + T_{1z}^{(S)} \eta_1 = 0$ on $z = 1$ to eliminate η_2 and find that $T_{2_z}^{(L)}(1) + \mathcal{L} T_2^{(L)}(1) = 0$; here we have used equation (3.23b).

At order ε^2 the governing system is the liquid has the form

$$\{\underline{\underline{L}} + R_c^{\frac{1}{2}} \underline{\underline{M}}\} \cdot \underline{\Psi}_2 - \begin{bmatrix} p_{2x} \\ p_{2y} \\ p_{2z} \\ 0 \end{bmatrix} = R_c^{\frac{1}{2}} \begin{bmatrix} P^{-1}\underline{v}_1 \cdot \nabla u_1 \\ P^{-1}\underline{v}_1 \cdot \nabla v_1 \\ P^{-1}\underline{v}_1 \cdot \nabla w_1 \\ \underline{v}_1 \cdot \nabla T_1^{(L)} \end{bmatrix} - \frac{1}{2} R_c^{-\frac{1}{2}} R_1 \underline{\underline{M}} \cdot \underline{\Psi}_1 \tag{3.30a}$$

$$\nabla \cdot \underline{v}_2 = 0. \tag{3.30b}$$

The boundary conditions at $z = 0$ are

$$u_2 = v_2 = w_2 = T_2^{(L)} = 0 \qquad \text{on } z = 0. \tag{3.30c}$$

The boundary conditions at z = 1 are obtained by referring the conditions on the deflecting interface to its mean position z = 1 and using the order ε conditions for simplifying the expressions. The final form requires a good deal of algebraic manipulation and leads to the following:

$$
\begin{aligned}
&u_2(x,y,1) = -\eta_1(x,y)u_{1_z}(x,y,1)\\
&v_2(x,y,1) = -\eta_1(x,y)v_{1_z}(x,y,1)\\
&w_2(x,y,1) = 0\\
&T_{2_z}^{(L)}(x,y,1) + \mathcal{L}\,T_2^{(L)}(x,y,1) = 0 \quad .
\end{aligned}
\tag{3.30d}
$$

We now apply the Fredholm alternative and take the scalar product of equation (3.30a) with $\underline{\Psi}_1$. From Davis and Segel (1968) we see that (i) the pressure gradient terms vanishes, (ii) the nonlinear term vanishes, (iii) the terms involving the operator inversion, using Green's theorem, of $\underline{\underline{L}} + R_c^{1/2}\,\underline{\underline{M}}$ vanish except for the boundary intergrals. In the latter terms we use conditions (3.21) and (3.30c,d) to reduce these. The results takes the form

$$
\frac{1}{2}\,R_c^{\frac{1}{2}}\,R_1\,\langle \underline{\Psi}_1,\ \underline{\underline{M}}\cdot\underline{\Psi}_1\rangle = -\eta_1\overline{\left[u_{1_z}^2(x,y,1)+v_{1_z}^2(x,y,1)\right]}\ . \tag{3.31}
$$

We now use the definitions of $\underline{\Psi}_1$ and $\underline{\underline{M}}$ from (3.24) and the scalar product (3.26) to rewrite equation (3.29) as follows:

$$
R_1 = -R_c^{\frac{1}{2}}\ \frac{\overline{\left[\eta_1\left(u_{1_z}^2+v_{1_z}^2\right)_{z=1}\right]}}{\int_0^1 \overline{w_1 T_1^{(L)}}\,dz}\ . \tag{3.32}
$$

Finally, we introduce the normal modes (3.16), use relation (3.22) and eliminate H_1 using form (3.23b) to obtain

$$R_1 = \frac{R_c^{\frac{1}{2}} \mathcal{L}^{-1} \left[D\, T_1^{(L)}(1)\right]\left[D^2 W_1(1)\right]^2}{k^4 \int_0^1 W_1\, T_1^{(L)}\, dz} \; \frac{\overline{\Phi(\Phi_x^2 + \Phi_y^2)}}{\Phi^2} \qquad (3.33)$$

The work of Schlüter, Lortz and Busse (1965) Segel (1965) and Busse (1967) have shown that stability considerations lead to the appearance of either roll cells or hexagons and that the nonlinear competition is contained in the following special form for Φ:

$$\Phi(x,y) = Y \cos\tfrac{1}{2}ky \cos\tfrac{1}{2}\sqrt{3}ky + Z \cos ky \;, \qquad (3.34)$$

where rolls have $Y = 0$, $Z \neq 0$ and hexagons have $Y = \pm 2Z$. The normalization (3.17) requires

$$\tfrac{1}{4} Y^2 + \tfrac{1}{2} Z^2 = 1 \qquad (3.35)$$

so that $Z = \pm\sqrt{2}$ for rolls and $Z = \pm\sqrt{2/3}$ for hexagons.

The integration giving the horizontal average, is zero for rolls so that $R_1 = R_1^{(R)} = 0$ in this case while for hexagons it gives $\pm \frac{1}{9}\sqrt{6}\, k^2$. Figure 7 shows $R_1 = R_1^{(H)}$ for hexagons with $Z > 0$ as a function of B. Here we have used the numerically computed eigenfunctions W_1 and $T_1^{(L)}$ to evaluate expression (3.33) and we have used the normalization $\max W_1(z) = 0.93848\, k_c^2(B)$.

At this stage we could obtain the order ε^2 solutions, examine the order ε^3 perturbation terms and formally obtain $R_2(B)$ for B arbitrary; this would then give us

$$R^{(H)} \sim R_c + R_1^{(H)} \varepsilon + R_2^{(H)} \varepsilon^2 \qquad (3.36a)$$

for hexagons and

$$R^{(R)} \sim R_c + R_2^{(R)} \varepsilon^2 \qquad (3.36b)$$

for rolls. However, if B is not small, there is no justification for the retention in equation (3.36a) of the term $R_2^{(H)} \varepsilon^2$ since it is obtained by perturbation theory in ε which makes it formally negligible compared to $R_1^{(H)} \varepsilon$. On the other hand if B is

small[+)], so that a double expansion in ε and B is permissible, than all three terms can be retained. Thus, it is then justifiable to write

$$R_2^{(H)}(B) \approx R_2^{(H)}(0) = C^2 \cdot R_c \left[0.89360 + 0.04959\ P^{-1} + 0.06787\ P^{-2}\right], \quad (3.37a)$$

$$R_2^{(R)}(B) \sim R_2^{(R)}(0) = C^2 \cdot R_c \left[0.69942 - 0.00472\ P^{-1} + 0.00832\ P^{-2}\right], \quad (3.37b)$$

$$R_c(B) \sim R_c(0) = 1707.762\ , \quad (3.37c)$$

$$k_c(B) \sim k_c(0) = 3.119 \quad (3.37d)$$

where

$$C^2 = R_c^{\frac{1}{2}} \int_0^1 W_1(z)\, T_1^{(L)}(z)\, dz = 2904.4\ . \quad (3.37e)$$

The values given in (3.37a,b) are computed by Schlüter et al. (1965); we have inserted factors R_c and C^2 to account for the differences in non-dimensionalization and eigenfunction normalization between Schlüter et al. and us. We do so in equations (3.38) below as well. For small B, $\mathscr{L}^{-1} = 0(B)$ so that formula (3.33) gives, consistent with Figure 7, that

$$R_1^{(H)}(B) \sim R_1^{(H)}(0) = -42.0\ R_c(0) B\ . \quad (3.37f)$$

From now on we use the symbol R_c to denote $R_c(0)$.

+) Equivalently, we could write $B = \bar{B}\varepsilon$ where $\bar{B} = 0(1)$ as $\varepsilon \to 0$ and perturb in the single parameter ε. In this case for hexagons we would get $R \sim R_c + (R_{20} + R_{21}\bar{B})\varepsilon^2$ where R_{20} would be equivalent to the B = 0 result of Schlüter et al. (1965) and R_{21} would be our $R^H{}_1(0)$; the results are thus identical.

3.3 Preferred Mode

The foregoing computation for steady convection leads to an infinite number of convective states, one for each Φ, which need to be distinguished by stability considerations. This has been done generally by Busse (1967) for cases where R_1 is small and generated by thermal variations in fluid properties. His stability analysis applies directly to our present work if B is small[+)] in which case four ranges of Rayleigh numbers exist for stable convective states. We can write these as follows:

$$
\begin{array}{lll}
\text{I.} & 0 < R < R_A = R_c - \dfrac{\left[R_1^{(H)}\right]^2}{4\,R_2^{(H)}} & \text{pure conduction only} \\
\text{II.} & R_A < R < R_c & \text{pure conduction or hexagonal convection} \\
\text{III.} & R_c < R < R_R = R_c + \dfrac{3R_2^{(R)}\left[R_1^{(H)}\right]^2}{C^4 R_c^2 L_2^2} & \text{hexagonal convection only} \\
\text{VI.} & R_R < R < R_B = R_c + \dfrac{\left[9R_2^{(H)} - 3C^2 R_c L_2\right]\left[R_1^{(H)}\right]^2}{C^4 R_c^2 L_2^2} & \text{hexagonal convection or roll convection} \\
\text{V.} & R > R_B & \text{roll convection only}
\end{array}
\qquad (3.38)
$$

where from Busse (1967) we have

$$L_2 = 0.29128 + 0.08147\,P^{-1} + 0.08932\,P^{-2}\,. \qquad (3.39)$$

+) The interface deflection and the phase changes give rise to new local time derivatives (in the kinematic and Stefan boundary conditions) compared to the classical case. When B is small, these terms do not alter the stability results of Busse (1967) nor the ranges listed above. However, if B is not small, then one does not know the result.

These ranges from the small B theory have been drawn in Figure 4 for $P \to \infty$. For purposes of clarity we have shown the curves for values of B larger than those appropriate for the perturbation theory. It is seen that the ranges divide the plane R versus B into sectors related to the observations though quantitative comparisons are not possible.

In range I, pure conduction is the only stable steady state. In range II, pure conduction is locally stable but there can be a jump transition to stable hexagonal convection as indicated in the bifurcation plot of equations (3.36) of Figure 8. Here a path $a \to b$ of increasing R results a jump to point c. If R increases further, hexagonal convection is maintained. However, if R is decreased along $c \to d$, then there is a jump down to pure conduction. Thus, abcd constitutes a hysteresis loop. Since $R_1 < 0$, the hexagons that occur have upflow at their centers. Hexagons having downflow at their centers are unstable. In range III, the same hexagons persist. In range IV both rolls and hexagons are stable while in range V only rolls can persist. Again the path a'b'c'd' constitute a hysteresis loop, this time involving jumps between hexagonal and roll convection.

3.4 Mean Interface Position

The nonlinear theory for small B gives ranges for stable hexagons, rolls or both as listed in (3.38). The theory shows that the first hexagons seen (as R is increased) should occur through a jump as shown in Figure 8. Thus jump occurs somewhere between $R = R_A$ and $R = R_c$ and has magnitude between $R_1^{(H)}/2R_1^{(H)}$ and $R_1^{(H)}/R_2^{(H)}$. Given such a jump in ε, there should be an accompanying jump in the mean position of the solidification interface.

We can examine this jump for small B by first solving for the order ε^2 mean temperature $\overline{T}_2^{(L)}$. It satisfies

$$D^2 \overline{T}_2^{(L)} = R_c^{\frac{1}{2}} D\,(W_1 T_1^{(L)}) \qquad (3.40a)$$

$$\bar{T}_2^{(L)}(0) = 0 \tag{3.40b}$$

$$D\bar{T}_2^{(L)}(1) + \mathcal{L}\,\bar{T}_2^{(L)}(1) = 0 \,. \tag{3.40c}$$

We solve system (3.40) to find that

$$\bar{T}_2^{(L)}(z) = R_c^{\frac{1}{2}} \left\{ \int_0^z W_1 T_1^{(L)} dz - \frac{1}{1+\mathcal{L}^{-1}} \left[\int_0^1 W_1 T_1^{(L)}\, dz \right] z \right\} . \tag{3.41}$$

We now average equation (3.29) over x and y to obtain

$$D\bar{T}_2^{(L)}(1) = -\mathcal{L}(\bar{\eta}_2 + \mathcal{L}\,\overline{\eta_1^2}) = -\mathcal{L}(\bar{\eta}_2 + \mathcal{L}^{-1}\left[DT_1^{(L)}(1)\right]^2) \tag{3.42}$$

where we have used forms (3.16a), (3.17) and (3.23b). We now combine equations (3.41) and (3.42) to obtain

$$\bar{\eta}_2 = \mathcal{L}^{-1}\left\{ \frac{R_c^{\frac{1}{2}}}{1+\mathcal{L}^{-1}} \int_0^1 W_1 T_1^{(L)} dz - \left[DT_1^{(L)}(1)\right]^2 \right\} \tag{3.43}$$

The relation (3.43) is plotted in Fig.9; for small B, $\bar{\eta}_2 \sim 579\ B$. Now, since $\eta \sim 1 + \varepsilon\eta_1 + \varepsilon^2\eta_2$, $\bar{\eta} \sim 1 + \varepsilon^2\bar{\eta}_2$ and ε jumps in the range

$$\left(\frac{1}{2}\,\frac{R_1^{(H)}}{R_2^{(H)}} \,,\ \frac{R_1^{(H)}}{R_2^{(H)}}\right)$$

then for $B \to 0$ the mean jump $\bar{\eta} - 1 = 0\,(B^3)$. Since $\bar{\eta}_2 > 0$, the onset of hexagonal convection is accompanied by a jump in mean thickness of the liquid layer.

3.5 Experimental/Theoretical Comparisons

We have posed a theory for convection initiated by a slight melting of a solid and the subsequent convection coupled to the deflection of an interface sustaining changes of phase.

The linearized stability theory shows that in spite of the interface temperature being known a priori, the disturbances see an imperfectly conducting solid medium at z = 1. Linearized theory gives $R_c(B)$ which decreases by about 12.5 % as B increases from zero to infinity. The critical wave-number $k_c(B)$ decreases by

about 9.7 % over the same range. These values are consistant with the experimental observations. For example our measurements of the hexagons in figure 3c gives $k = 3.0 \pm 0.2$ for $R = 3300$ and $B = 0.36$ while the linear theory for $R = R_c(0.36) \approx 1520$ and the same B gives $k \approx 2.9$. The rolls of figure 3a have $k = 2.5 \pm 0.1$ for $R = 7500$ and $B = 0.03$ qualitatively consistent with the wavenumber decreasing with increasing $R > R_c$.

The nonlinear theory for small B gives ranges for stable hexagons, rolls or both as listed in (3.38). The range of predicted hexagons approaches zero with B consistent with the experimental observation that only roll cells are seen for small enough B ($B \approx 0.05$). For the value $B = 0.05$ stable hexagons should be in the range

$$-4.2 \times 10^{-4} < \frac{R-R_c}{R_c} < 1.3 \times 10^{-1} \qquad (3.44)$$

which would be difficult to see by present techniques. However, when B is large the range of stable hexagons should be large consistent with the experimental observation that for B large enough ($B = 0.16$) well formed hexagons or mixed polygonal states are always seen. For the value $B = 0.16$ stable hexagons should be in the range

$$-4.3 \times 10^{-3} < \frac{R-R_c}{R_c} < 1.3 \ . \qquad (3.45)$$

This range significantly exceeds the expected range of validity at our perturbation theory so that hexagons would be predicted "always"!

The theory shows that the first hexagons seen should be present due to a jump from the conduction state. Figure 8 shows a bifurcation diagram of equations (3.36) for hexagons and rolls. As R is increased, the pure conduction state loses stability through a jump of magnitude between $\frac{1}{2} R_1^{(H)}/R_2^{(H)}$ and $R_1^{(H)}/R_2^{(H)}$, which is $O(B)$ for small B. We have no experimental observations of such jumps in the present set-up since viewing from the side of a thin, wide layer is difficult. However, in a subsequent experi-

ment designed to focus on side-wall effects we have used identical materials but now a chamber having depth 10 mm and horizontal dimensions 20 mm x 200 mm. In these experiments B = 5.0 and we observe from the side a rapid jump in the mean position of the interface upon the onset of convection; the liquid layer doubles its thickness at the onset of convection. This is not an effect of changes of volume of the material upon solidification but one of the dynamical consequences of subcritical bifucation.

We note that there is an aternative mechanism for the creation of hexagonal patterns as discussed by Palm (1960), Segel and Stuart (1962), Busse (1967) and Davis and Segel (1968). Here thermal variations, say $\Delta\mu$, across the liquid layer, of each fluid property μ, having mean value μ_o, lead to R_1 proportional $\Delta\mu/\mu_o$. On one hand, cyclohexane closely satisfies the conditions of the Boussinesq approximations so that $\Delta\mu/\mu_o$ is very small within the temperature change $T_o-T_s \simeq 1$ K. On the other hand since T_o-T_s is fixed in the present experiment, independent of B, theories based on non-Boussinesq effects would predict a range of hexagons independent of B contrary to our observations. Thus, such non-Boussinesq mechanisms are negligible in the present case.

4. Conclusions

In this paper we have examined a single component liquid that solidifies at a known temperature T_s. The configuration involves a layer heated from below and cooled from above. A slight melting of the solid initiates steady thermal convection coupled to the deflection of an interface at which the changes in phase occur.

We have discussed an experiment in which large values of B (the ratio of solid to liquid thicknesses) lead to hexagonal convection that is readily observed while small values of B lead to only to line patterns. Presumably, hexagons exist in a Rayleigh number range too small to resolve experimentally.

We have discussed a theory for which small values of B are required since the perturbation theory is questionable when B is large.

We have compared experimental observation with theoretical prediction and found very good qualitative agreement in that (i) hexagonal convection and solid-liquid interface patterns predominate at large B while two-dimensional convection and patterns are seen at small B, (ii) the wave-number of the cells is governed by a stability theory, (iii) the onset of hexagonal convection is accompanied by a jump in the mean position of the solid-liquid interface so that the liquid depth suddenly increases.

The above agreement gives confidence that the coupled convective/phase-change system considered gives rise to hexagonal symmetries and that these states are driven by alterations in heat transfer at the interface due to interfacial deformation. Further, the prediction of upflow in the centers of the hexagonal cells fits ones view that the phenomena are well-modeled by the theory. This mechanism should be present in other more complicated solidification systems.

Acknowledgement

The authors gratefully acknowledge the assistance of P. Damm during the performance of the experiments.

References

Busse, F.; 1967, The Stability of Finite Amplitude Cellular Convection and its Relation to an Extremum Principle; J. Fluid Mech. 30, 625-649.

Coriell, S.R.; Cordes, M.R.; Boettinger, W.J.; Sekerka, R.F.; 1980, Convective and Interfacial Instabilities During Unidirectional Solidification of a Binary Alloy; J. Cryst. Growth 49, 13.

Coriell, S.R.; Sekerka, R.F.; 1982, Effect of Convective Flow on Morphological Stability; PCH Physico Chemical Hydrodynamics 2, 281-293.

Davis, S.H., Segel, L.A.; 1968, Effects of Surface Curvature and Property Variation on Cellular Convection; Phys. Fluids 11, 470-476.

Farhadieh, R., Tankin, R.S.; 1975, A Study of the Freezing of Sea Water; J. Fluid Mech. 71, 293-304.

Fischer, K.M.; 1981, The Effects of Fluid Flow on the Solidification of Industrial Castings and Ingots; PCH Physico Chemical Hydrodynamics 2, 311-326.

Foster, T.D.; 1969, Experiments on Haline Convection Induced by the Freezing of Sea Water; J. Geophys. Res. 74, 6967-6974.

Hurle, D.T.J.; Jakeman, E.; Wheeler, A.A.; 1982, Effect of Solutal Convection on the Morphological Stability of a Binary Alloy; J. Crystal Growth 58, 163-179.

Hurle, D.T.J., Jakeman, E., Wheeler, A.A.; 1983, Hydrodynamic Stability of the Melt During Solidification of a Binary Alloy; Phys. Fluids 23, 624-626.

Hurle, D.T.J., Jakeman, E.; 1981, Introduction to the Techniques of Crystal Growth; PHC Physico Chemical Hydrodynamics 2, 237-244.

Marshall, R.; 1981, Experimental Experience with the ASHRAE/NBS Procedures for Testing a Phase Change Thermal Storage Device; in: International Conference on Energy Storage, Brighton, April 1981, Vol. 1, 129-143.

Mihaljian, J.M. 1962, A Rigorous Exposition of the Boussinesq Approximation Applicable to a Thin Layer of Fluid; Astrophys. J. 136, 1126-1133.

Mullins, W.W., Sekerka, R.F.; 1964, Stability of a Planar Interface During Solidification of a Dilute Binary Alloy; J. Appl. Phys. 35, 444-451.

Nield, D.A.; 1968, The Rayleigh-Jeffreys Problem with Boundary Slab of Finite Conductivity; J. Fluid Mech. 32, 393-398.

Palm, E.; 1960, On the Tendency Towards Hexagonal Cells in Steady Convection; J. Fluid Mech. 8, 183-192.

Pantaloni, J.; Velarde, M.G.; Bailleux, R.; Guyon, E.; 1977, Sur la convection cellulaire dans les sels fondus pres de leur point de solidification; Comptes Rendus Hebdomadaires Des Seances De L`Academie Des Sciences, 285, Ser.B, 275-278.

Saitoh, T.; Hirose, K.; 1980, Thermal Instability of Natural Convection Flow over a Horizontal Ice Cylinder Encompassing a Maximum Density Point; J. Heat Transfer 102, 261-266.

Saitoh, T.; Hirose, K.; 1982, High Rayleigh Number Solutions to Problems of Latent Heat Thermal Energy Storage in a Horizontal Cylinder Capsule; J. Heat Transfer 104, 545-553.

Schlüter, A.; Lortz, D.; Busse, F.; 1965, On the Stability of Steady Finite Amplitude Convection; J. Fluid Mech. 23, 129-144.

Segel, L.A.; Stuart, J.T.; 1962, On the Question of the Preferred Mode in Cellular Thermal Convection; J. Fluid Mech. 13, 289-306.

Segel, L.A.; 1965, The Nonlinear Interaction of a Finite Number of Disturbances to a Layer of Fluid Heated From Below; J. Fluid Mech. 21, 359-384.

Sriranganathan, R.; Wollkind, D.J.; Oulton, D.B.; 1983, A Theoretical Investigation of the Development of Interfacial Cells During the Solidification of a Dilute Binary Alloy: Comparison with the Experiments of Morris and Winegard; J. Crystal Growth 62, 265-283.

Wollkind, D.J.; Segel, L.A.; 1970, A Nonlinear Stability Analysis of the Freezing of a Dilute Binary Alloy; Phil. Transactions, Roy. Soc. London A268, 351-380.

Wollkind, D.J.; Raissi, S.; 1974, A Nonlinear Stability Analysis of the Melting of a Dilute Binary Alloy; J. Crystal Growth 26, 277-293.

Yen, Yin-Chao; 1980, Free Convection Heat Transfer Characteristics in a Melt.Water Layer; J. Heat Transfer 102, 550-556.

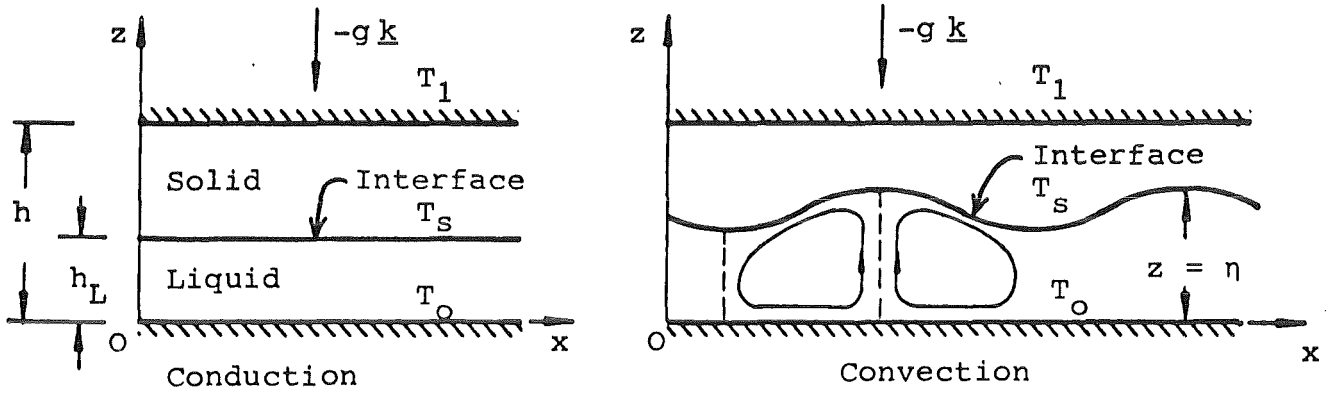

Fig. 1 Schematic drawing of partially solidified liquid layer.

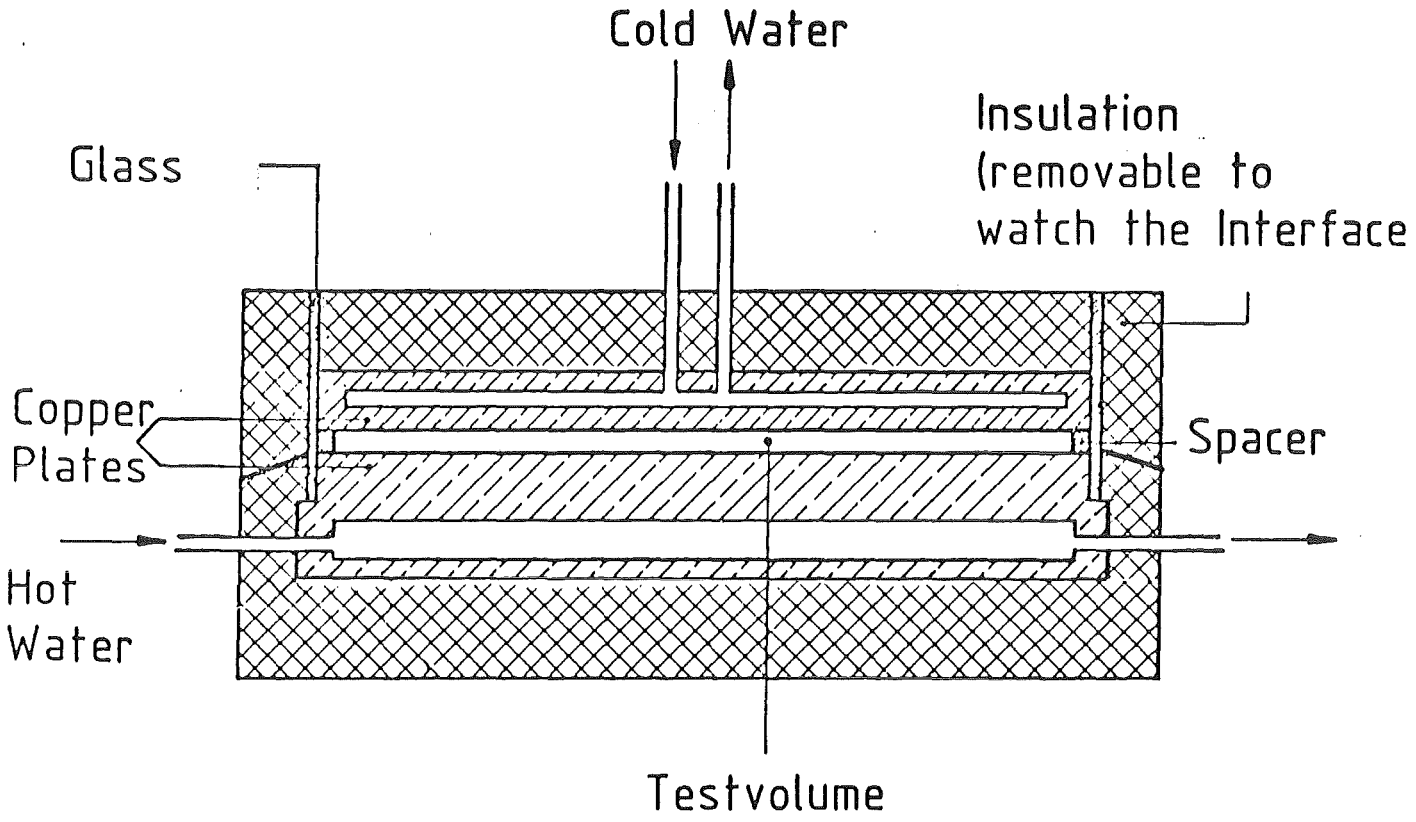

Fig. 2 Experimental apparatus, layer height 4.18 mm and 5.04 mm, layer width and depth 287 mm.

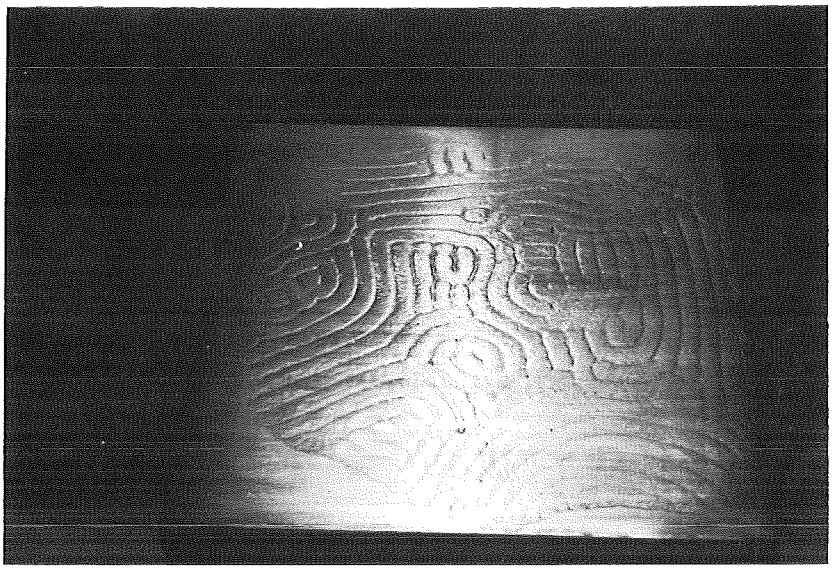

a)

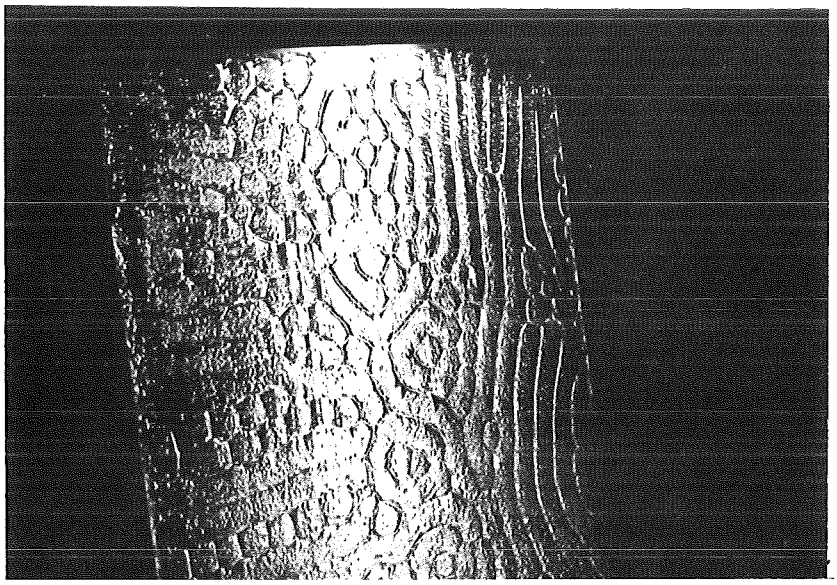

b)

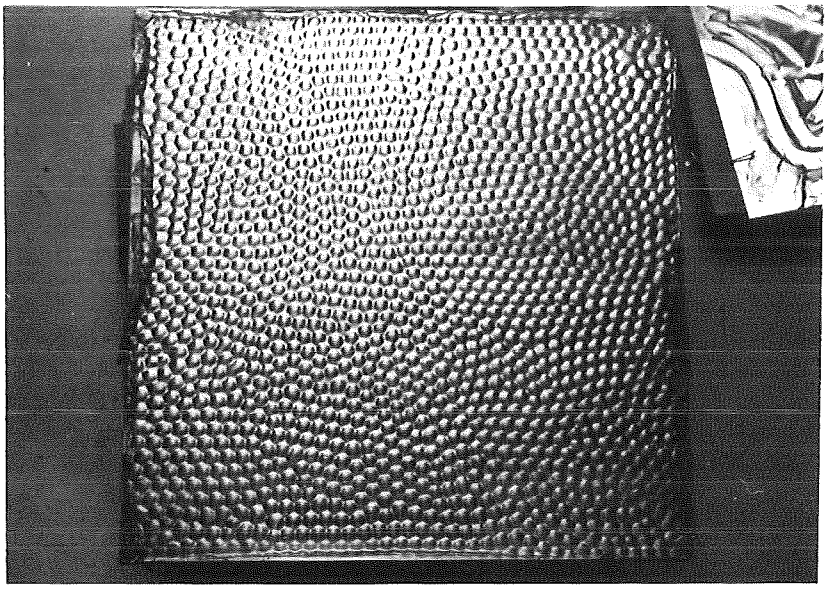

c)

Fig. 3 Photographs of corrugated "ice" surfaces a) hexagonal pattern, b) mixed hexagonal-line pattern) c) line pattern.

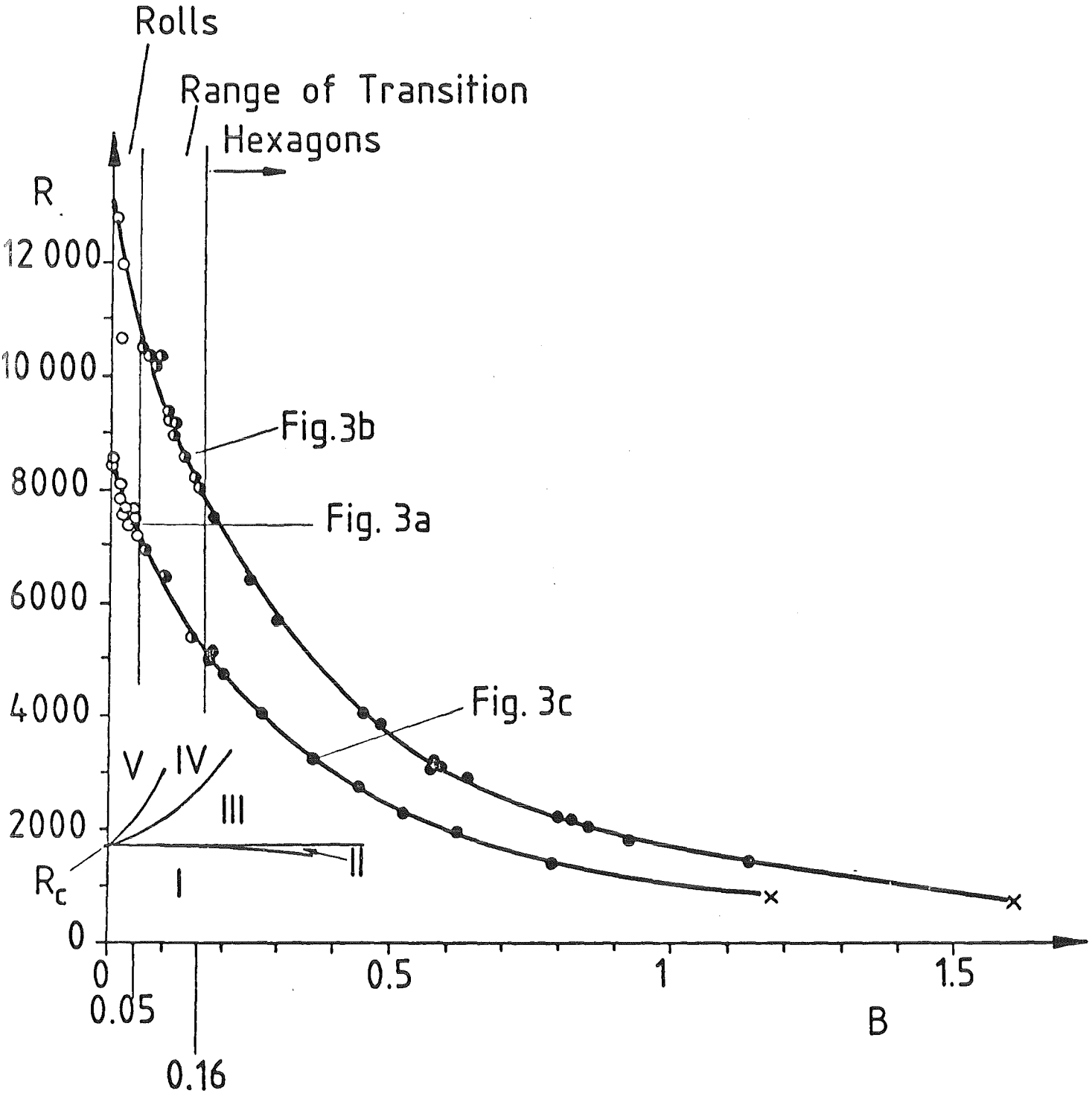

Fig. 4 Regime diagram on the R-B plane: lables I-V refer to critical values listed in (3.38); o denote rolls, ◍ denote rolls and polygons, ● denote hexagons, and x denotes states of rest.

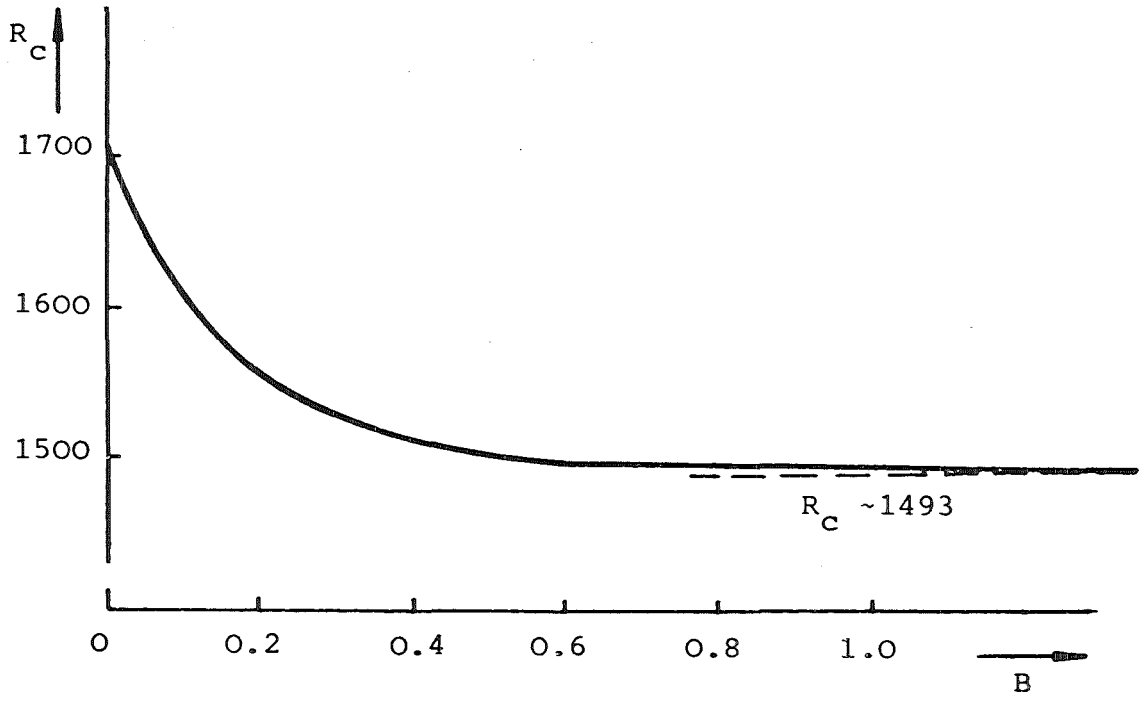

Fig. 5 Critical Rayleigh number as a function of the Biot number.

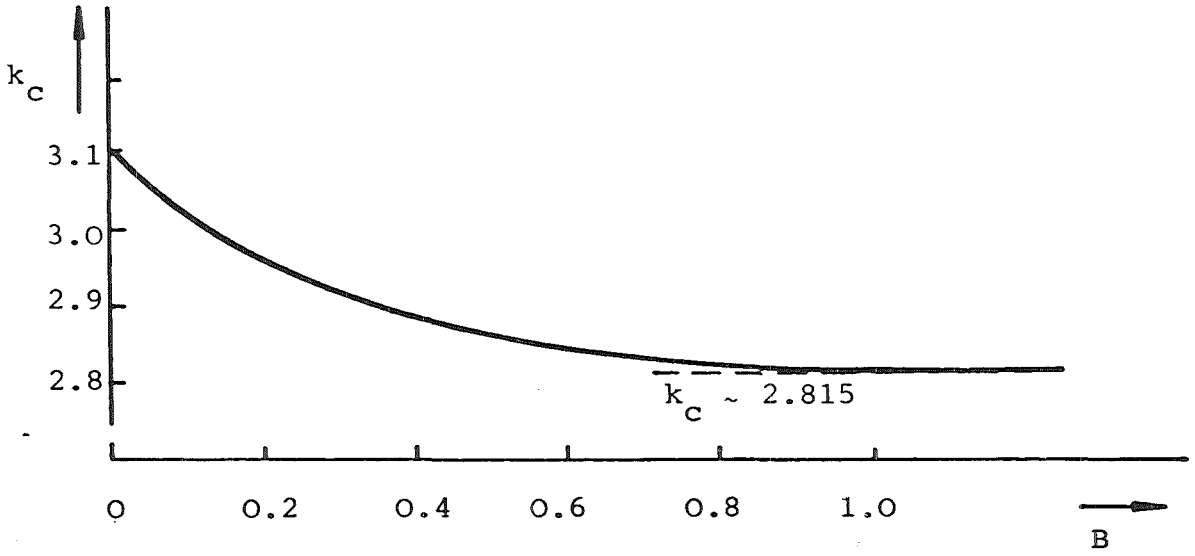

Fig. 6 Critical wave number as a function of the Biot number.

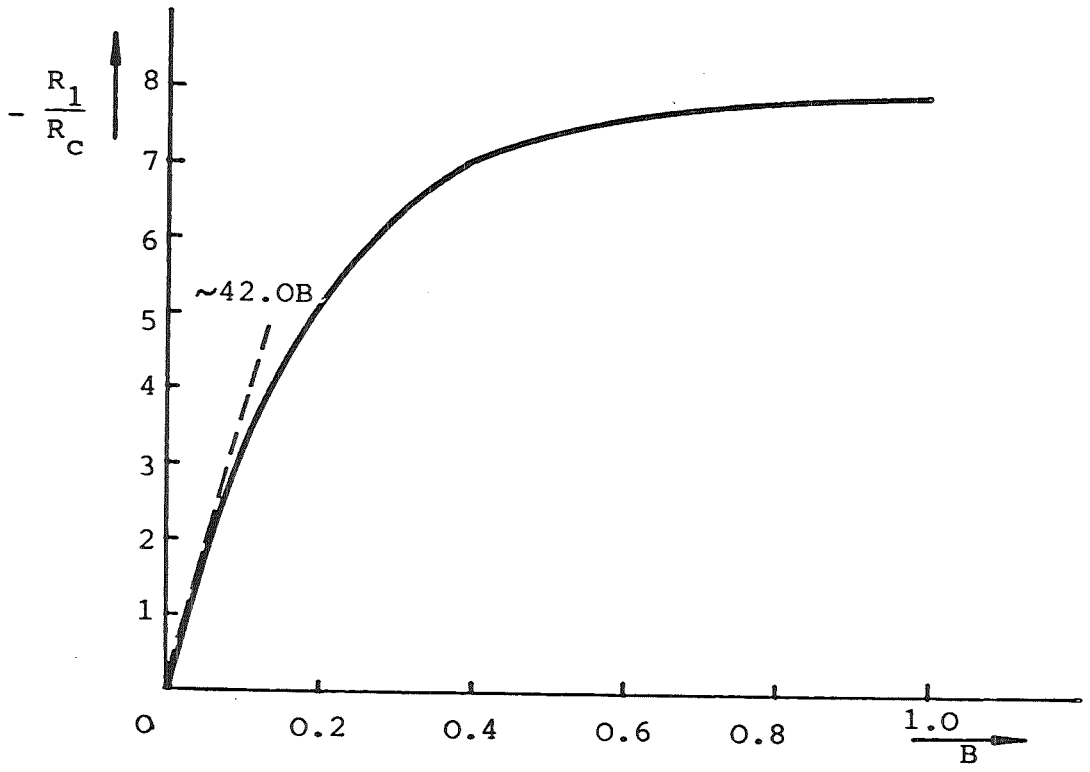

Fig. 7 Normalized first order correction term of the Rayleigh number as a function of the Biot number.

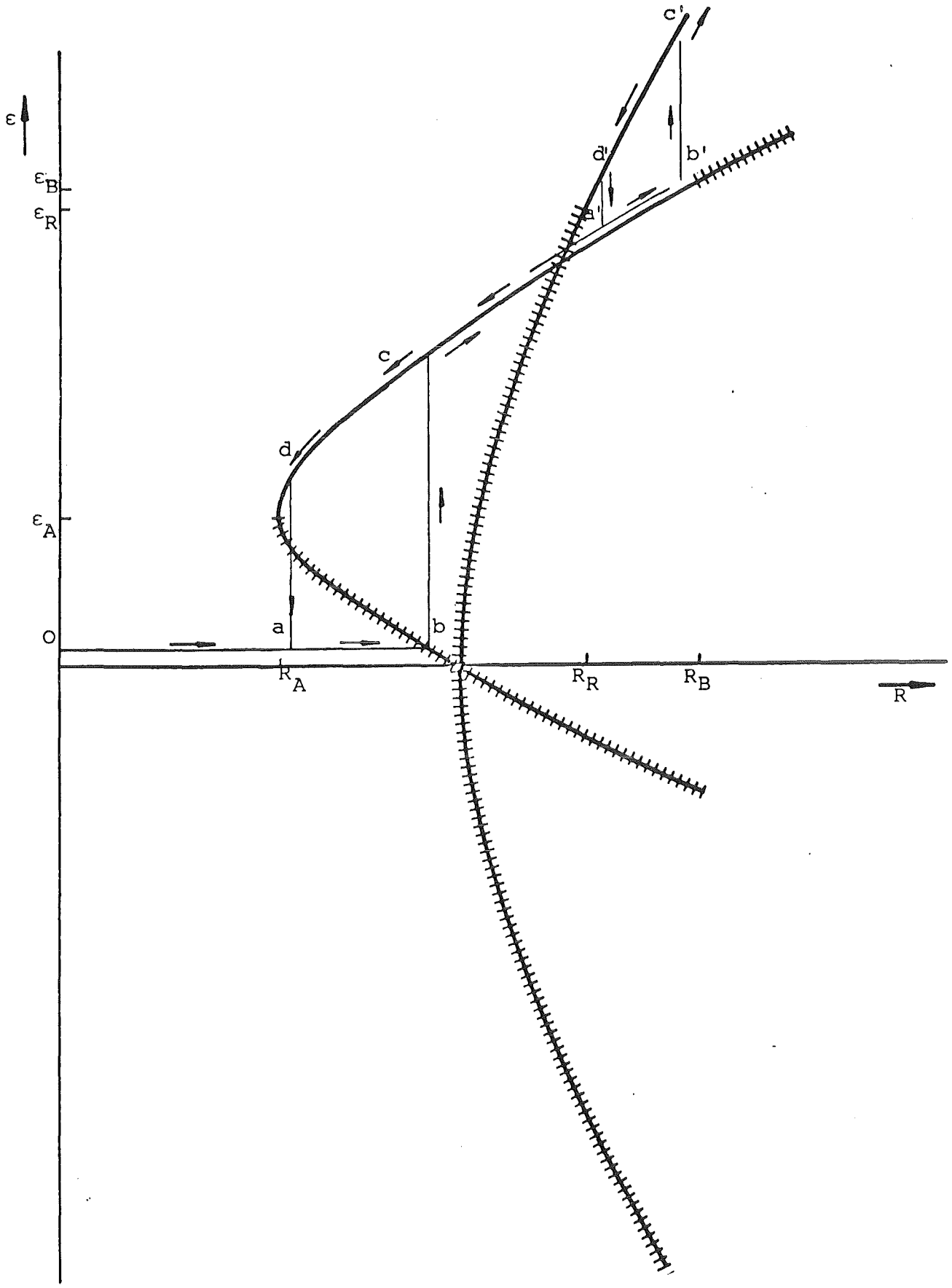

Fig. 8 Qualitative sketch of the dependence of the amplitude on the Rayleigh number for rolls and hexagons and bounds of stability, hatched curves mark the unstable branches of the roll and hexagonal solutions.

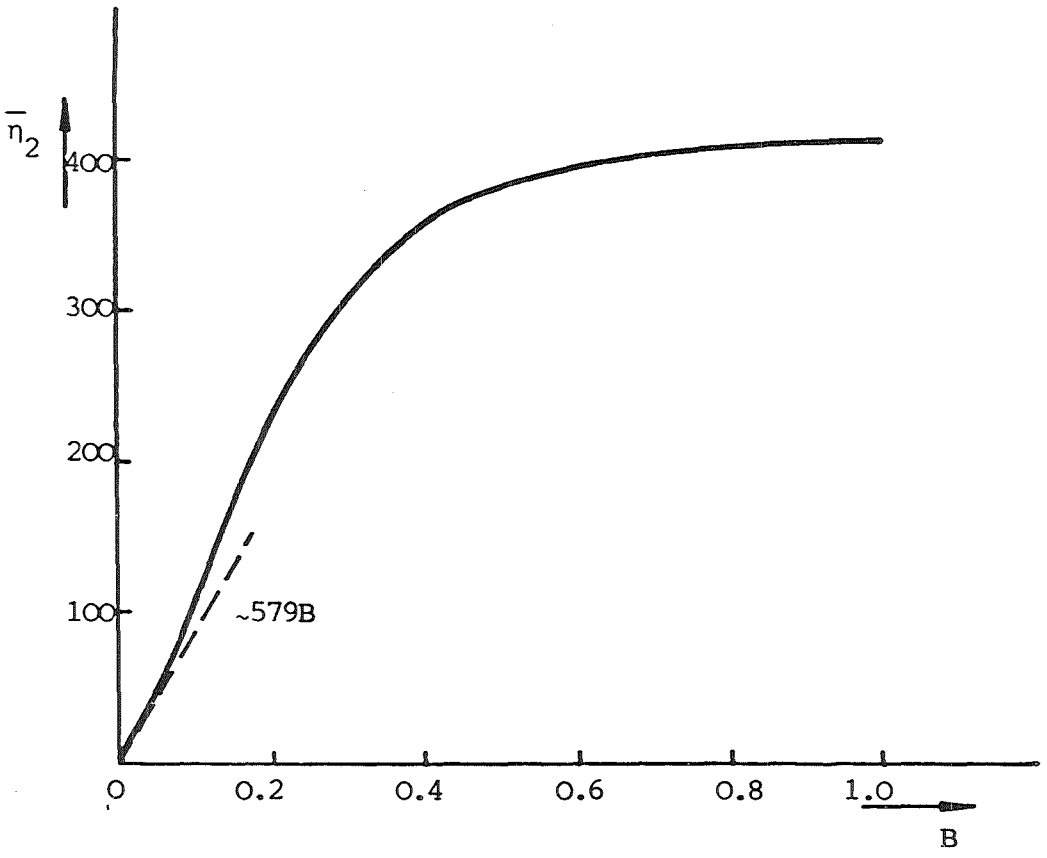

Fig. 9 The second order correction term for the average layer height as a function of the Biot number.